Stellar Turbulent Convection: A Selfconsistent Model

V. M. Canuto [1], I. Goldman[2,3,4] and I. Mazzitelli [5]

ABSTRACT

We present a selfconsistent model for stellar turbulent convection which is similar in spirit to the CM model (Canuto & Mazzitelli 1991) since it accounts for the full spectrum of the turbulent eddies rather than only one eddy, as done in the mixing length theory (MLT). The model differs from the CM model in the treatment of the rate of energy input $n_s(k)$ from the source that generates the turbulence. In the present model, $n_s(k)$ is controlled by both the *source* and *the turbulence* it ultimately generates, thus ensuring a selfconsistent modeling of the turbulence. This improves the CM model in which $n_s(k)$ was taken to be equal to the growth rate of the *linear* unstable convective modes.

However, since the formulation of a selfconsistent treatment is far from simple, we were forced to use a representation of the nonlinear interactions less complete than the one in the CM model. The ensuing equations were solved numerically for a wide range of convective efficiencies. The results are the convective flux, the mean square turbulent velocity, the root mean squared turbulent pressure and the turbulent viscosity.

We implemented the model in the ATON stellar structure code and computed the evolution of a solar model. The results are generally similar to those of the CM model and thus quite different from the MLT. The present model requires a smaller overshoot into the upper radiative zone than does the CM model,

[1]NASA Goddard Institute for Space Studies, 2880 Broadway, New York, NY 10025, USA, email: acvmc@nasagiss.giss.nasa.gov

[2]School of Physics and Astronomy, Sackler Faculty of Exact Sciences, Tel Aviv University, Tel Aviv 69978, Israel, email: goldman@plato.tau.ac.il

[3]Visiting Scientist, Department of Condensed-Matter Physics, Faculty of Physics, Weizmann Institute of Science, Rehovot 76100, Israel

[4]Visiting Scientist, Harvard–Smithsonian Center For Astrophysics, 60 Garden Street, Cambridge, MA 02138, USA

[5]Istituto di Astrofisica Spaziale, CNR, CP 67, 00044 Frascati, Italy, email: aton@hyperion.ias.fra.cnr.it

in accord with recent empirical estimates. Application to POP II stars and comparison with the very metal-poor globular cluster M68 yields an age in the range $11 \div 12$ Gyr. This is somewhat younger than the CM age, which in turn is younger than the corresponding MLT age, a result of possible cosmological interest.

Subject headings: convection — stars: interiors — stars: evolution — Sun: interior — turbulence

1. Introduction

Recently, Canuto & Mazzitelli (1991, CM) proposed an improved model for stellar convection. Being derived from a turbulence model, it takes into account the contribution of the full spectrum of the turbulent convective eddies, to the convective flux. In stellar interiors the microscopic viscosity is very small compared to the turbulent viscosity, implying that the turbulent spectrum spans many decades in wavenumber space. Therefore, in this respect, the CM model represents a significant improvement over the mixing length theory approach (MLT) which is a one eddy (the largest) approximation to the spectrum. Moreover, in the CM model, the turbulent mixing length scale is the depth z, so there is no need for an adjustable free parameter like the MLT α-parameter. The resulting convective fluxes are higher than those of the MLT for high convective efficiencies, and smaller than them for low efficiencies. The model performs better than the MLT when applied to stellar structure (D'Antona & Mazzitelli, 1994; Mazzitelli, D'Antona & Caloi 1995, Stothers & Chin 1995, Althaus & Benvenuto 1996), helioseismology (Baturin & Mironova 1995, Monteiro et al. 1995, Antia & Basu 1995) and stellar atmospheres (Kupka 1995).

In the CM model, the turbulence spectral function $E(k)$ is determined by the timescale controlling the energy input from *buoyancy*, that is, the *source* that generates the turbulence. This timescale is expected to depend on the parameters of the source as well as on the *turbulence spectrum* itself. The quantification of the latter dependence, within the CM model, is far from obvious. Thus, CM (1991) assumed that the above timescale can be approximated by the inverse of the growth rate of the unstable modes of the *linearized* equations. By construction, the latter depends only on the source and is *independent* of the *turbulence* it generates. The linear rate was used also by Canuto Goldman and Chasnov (1987,CGC) who, generalizing the work of Canuto and Goldman (1985), proposed a model for fully developed turbulence. The linear rate was also employed by Hartke Canuto & Dannevik (1988) in the framework of a DIA (Direct Interaction Approximation) model for

turbulent convection and by Canuto, Cheng, Hartke, & Schilling (1991) for EDQNM (Eddy Damped Quasi-Normal Markovian) models.

The rate of energy input in the CM model must be improved since a fully developed turbulence is expected to regulate the energy input from source (buoyancy). The lack of feedback from the turbulence on the energy input, prevents the model from being selfconsistent. However, because of the complex structure of the EDQNM closure, the implementation of a selfconsistent rate into the formalism of the CM model is not simple. Thus, we were forced to simplify the structure of the nonlinear interactions, so as to be able to formulate a workable selfconsistent treatment.

In modeling the nonlinear interactions, we follow the work of CGC (1987). However, in the present model we generalize the definition of the eddy correlation timescale, thus correcting some shortcomings in the physics involved, and leading to an improved closure. The resulting effective rate of energy input from the source (buoyancy) depends now on both the *source* and the *turbulence*. As stated, the present approach is complementary to that of the CM model. Here, the focus is on the selfconsistent rate of energy input and not on the closure, which is much simpler than that of the CM model.

In spite of the highly nonlinear structure of the model equations, it is possible to solve them *directly* with no need for iterations. This reduced considerably the amount of numerical work required, and allowed for an exploration of the model for a wide range of values of the convective efficiency, S, defined in equation (51). For each value of S we obtained the spectral function which determines the turbulence bulk quantities. Thus, we computed, as functions of S, the convective flux, the turbulent viscosity, the turbulent mean squared velocity and the root mean squared turbulent pressure.

We have applied the new model to the main sequence evolution of a solar model as well as to the evolutions of an extreme POP II chemical composition (Y=0.23, Z=10^{-4}) stars with $M \leq 0.9\ M_{\odot}$. The results are generally similar to those of the CM model. However, the new model has the advantage that the overshoot required to fit the solar model is much smaller, in accord with recent empirical estimates, and the ages of globular clusters are also somewhat smaller than the corresponding ages in the CM model (which in turn are smaller than those derived within the MLT framework).

2. The Model

2.1.   The Rate Controlling Energy Input from the Source

Let us consider a fully developed stationary turbulent convection characterized by the spectral functions $F(k)$, $G(k)$ and $H(k)$, of the turbulent velocity, temperature fluctuations and the turbulent convective flux, respectively. Before doing so, we write the dynamical time-dependent equations obeyed by these spectral functions (Yamaguchi 1963).

$$\frac{\partial}{\partial t} F(k) + \nu k^2 F(k) = g\alpha H(k) + T_F(k) \ , \tag{1}$$

$$\frac{\partial}{\partial t} G(k) + \chi k^2 G(k) = \beta H(k) + T_G(k) \ , \tag{2}$$

and

$$\frac{\partial}{\partial t} H(k) + (\nu + \chi)k^2 H(k) = \beta\tau(k)F(k) + g\alpha\tau G(k) + T_H(k) \ , \tag{3}$$

where T_F, T_G, and T_H denote the nonlinear transfer terms for the turbulent velocity, temperature, and convective flux. Here, g is the gravitational acceleration, α is the coefficient of thermal volume expansion at constant pressure (equaling T^{-1} for an ideal gas), β is the superadiabatic temperature gradient, ν is the microscopic viscosity, and χ is the microscopic thermometric conductivity appearing in the expression for the conductive flux

$$F_{cond} = -c_p \rho \chi \frac{dT}{dz} \ . \tag{4}$$

In stellar interiors, the dominant conductive flux is the radiative flux and thus χ is the radiative thermometric conductivity. The function $\tau(k)$ is given by

$$\tau(k) = \frac{x(k)}{1 + x(k)} \tag{5}$$

with $x(k) = k_h^2/k_v^2$ measuring the anisotropy of the eddy corresponding to the wavenumber k. Here, k_h and k_v stand for the horizontal and vertical wavenumbers, respectively (the vertical direction is that of the gravitational acceleration).

In equation (1), $g\alpha H(k)$ plays the role of the energy source driving the velocity fluctuations. More precisely, it equals the rate of energy per unit mass and per unit wavenumber, fed to the turbulence velocity field at wavenumber k. The term $\nu k^2 F(k)$ is the rate of energy per unit mass and unit wavenumber dissipated at k by the microscopic viscosity, while $-T_F(k)$ represent the rate of energy per unit mass and unit wavenumber

transferred to wavenumbers *other* than k. Analogous interpretations apply to equation (2) which describes the temperature fluctuations field.

As stated above, we are interested in stationary turbulence. Thus, in equations (1)–(3) we set the time derivatives of the spectral functions equal to zero. Following CGC (1987), we assume that

$$\frac{T_H(k)}{H(k)} = \frac{T_F(k)}{F(k)} + \frac{T_G(k)}{G(k)} \tag{6}$$

which equations (1), (2), and (3) show to be equivalent to the assumption:

$$H(k) = \left(\tau(k)F(k)G(k)\right)^{1/2}. \tag{7}$$

For equation (7) to be satisfied, the velocity and temperature fluctuations, at any k, must be in phase. This is expected to be the case for turbulent convection where the temperature plays the role of an *active scalar* whose fluctuations *drive* the velocity fluctuations.

We adopt the simplifying assumption that the transfer terms in equations (1) and (2) describe transfer from small to large wavenumbers only (from large spatial scales to small ones). While justified in three dimensional turbulence where energy flows predominantly from large to small scales, this simplifying assumption neglects non-local interactions (in k space) that give rise to reverse transfer (backscatter).

Denoting by k_0 the wavenumber corresponding to the largest eddy, we shall represent the transfer as

$$\int_{k_0}^{k} T_F(k')dk' = -\nu_t(k)y(k) \tag{8}$$

where

$$y(k) = \int_{k_0}^{k} F(k')k'^2 dk' \tag{9}$$

is the mean squared turbulent vorticity and $\nu_t(k)$ is the turbulent viscosity at wavenumber k, exerted by all eddies of smaller size (larger k). As such, it is expressed as an integral with limits k and ∞. We shall return later to the definition of the integrand. Similarly,

$$\int_{k_0}^{k} T_G(k')dk' = -\chi_t(k)w(k) \tag{10}$$

where

$$w(k) = \int_{k_0}^{k} G(k')k'^2 dk' \tag{11}$$

is the analog to the mean squared turbulent vorticity and $\chi_t(k)$ is the turbulent conductivity at wavenumber k exerted by all eddies of smaller size (larger k). With these closures, we obtain by integrating equations (1) and (2)

$$g\alpha \int_{k_0}^{k} H(k')dk' = \Big(\nu + \nu_t(k)\Big)y(k) \; , \tag{12}$$

and

$$\beta \int_{k_0}^{k} H(k')dk' = \Big(\chi + \chi_t(k)\Big)w(k) \; . \tag{13}$$

The last two equations allow us to express the spectral function $G(k)$ in terms of $F(k)$. We obtain

$$G(k) = \frac{\beta}{g\alpha}\lambda(k)F(k) \; , \tag{14}$$

with

$$\lambda(k) = \frac{\Big(y(k)\Sigma_t(k)\Big)'}{y'(k)} \; , \tag{15}$$

$$\Sigma_t(k) = \frac{\nu + \nu_t(k)}{\chi + \chi_t(k)} \; , \tag{16}$$

where a prime denotes a differentiation with respect to k. Substituting equation (14) in equation (7) yields

$$H(k) = \left(\frac{\beta}{g\alpha}\tau(k)\lambda(k)\right)^{1/2} F(k) \; . \tag{17}$$

Thus, once $F(k)$ is known so are $G(k)$ and $H(k)$, implying that one needs to solve only for the spectral function $F(k)$. In order to do so, let us return to equation (12) and express $H(k)$ in terms of $F(k)$ using equation (17). We obtain

$$\int_{k_0}^{k} \Big(n_s(k') + \nu k'^2\Big)F(k')dk' = \Big(\nu + \nu_t(k)\Big)y(k) \tag{18}$$

where $n_s(k)$ is the shorthand abbreviation

$$n_s(k) \equiv -\nu k^2 + \left(g\alpha\beta\tau(k)\lambda(k)\right)^{1/2} , \tag{19}$$

whose dimension are inverse time. The combination $n_s(k) + \nu k^2$ plays, in equation (18), the role of the inverse of the timescale controlling the energy input into the turbulence at wavenumber k from the source (buoyancy in the present case). More specifically, the *net rate of energy input* from the source per unit mass and unit wavenumber, at k, is $n_s(k)F(k)$.

It is obvious, from equation (19), that $n_s(k)$ depends on the *source* (buoyancy) and on the *turbulent state*. Thus, it conforms with the requirements discussed in §1. In what follows we show that equations (18) and (19) allow us to express $n_s(k)$ in terms of the turbulent viscosity $\nu_t(k)$. First, differentiate equation (18) with respect to k. The result is

$$n_s(k) - \nu_t(k)' \frac{y(k)}{F(k)} = \nu_t(k)k^2 . \tag{20}$$

Next, use equations (15), (20) and the definition of y(k), equation(9), to get

$$\lambda(k) = \Sigma_t(k) + \frac{\Sigma_t(k)'}{k^2\nu_t(k)'}\left(n_s(k) - \nu_t k^2\right) . \tag{21}$$

With the help of equation (19), we transform equation (21) into a second order algebraic equation for $\lambda(k)$:

$$\lambda(k) = \Sigma_t^2(k)\frac{\chi_t'}{\nu_t'} + \left(g\alpha\beta\tau(k)\lambda(k)\right)^{1/2}k^{-2}\frac{\Sigma_t'}{\nu_t'} , \tag{22}$$

whose positive solution is

$$\lambda(k) = \frac{1}{2}\left(g\alpha\beta\tau(k)\right)^{1/2}k^{-2}\frac{\Sigma_t'}{\nu_t'}\left(1 + \left(1 + \frac{4k^4}{g\alpha\beta\tau}\left(\frac{\Sigma_t}{\Sigma_t'}\right)^2\chi_t'\nu_t'\right)^{1/2}\right) . \tag{23}$$

We adopt a relation between $\chi_t(k)$ and $\nu_t(k)$

$$\chi_t(k) = \left(\chi^2 + \sigma_t^{-2}\nu_t^2(k)\right)^{1/2} - \chi \tag{24}$$

so that, as in CGC (1987), $\nu_t(k)/\chi_t(k)$ equals the constant σ_t for large Pecle numbers, $Pe = \nu_t(k)/\chi$, while $\nu_t(k)/\chi_t(k) = 2\sigma_t^2\chi/\nu_t(k)$, for small Pe. Using equation (24) to express Σ_t and χ_t in terms of ν_t, equation (23) now takes the form

$$\lambda^{1/2}(k) = \frac{1}{2}(g\alpha\beta)^{1/2}\chi^{-1}\tau^{1/2}(k)k^{-2}\frac{B(k)}{A(k)} \tag{25}$$

with

$$A(k) = \left(1 + \sigma_t^{-2}\nu_t^2(k)\chi^{-2}\right)^{3/2} , \tag{26}$$

and

$$B(k) = 1 - \frac{\nu\nu_t(k)}{\sigma_t^2\chi^2} + \left(\left(1 - \frac{\nu\nu_t(k)}{\sigma_t^2\chi^2}\right)^2 + A(k)\frac{4k^4\nu_t(k)\left(\nu + \nu_t(k)\right)^2}{g\alpha\beta\chi\sigma_t^2\tau(k)}\right)^{1/2} . \tag{27}$$

With this $\lambda(k)$, $n_s(k)$ of equation (19) becomes

$$n_s(k) = -\nu k^2 + \frac{g\alpha\beta}{2\chi}\frac{\tau(k)}{k^2}\frac{B(k)}{A(k)} . \tag{28}$$

Thus, we succeeded in expressing $n_s(k)$ in terms of the turbulent viscosity $\nu_t(k)$, even though the latter *is still unspecified*.

2.2. The Eddy-Correlation Timescale

In order to solve equation (18) (or equivalently equation (20)) we need an additional relation between the turbulent viscosity $\nu_t(k)$ and the spectral function $F(k)$. Without loss of generality, $\nu_t(k)$ can be written as

$$\nu_t(k) = \int_k^\infty \frac{F(k')}{n_c^*(k')}dk' \tag{29}$$

where $n_c^*(k)$ has the dimensions of an inverse time. In order to determine $n_c^*(k)$ let us focus on its physical meaning. Differentiation of equation (29) yields that the turbulent viscosity contributed by eddies in the wavenumber interval $(k, k + dk)$ is

$$d\nu_t = n_c^*(k)^{-1}F(k)dk . \tag{30}$$

Thus, $n_c^*(k)$ is proportional to the inverse of the eddy-correlation timescale at wavenumber k, or heuristically, the inverse of the timescale for the eddy breakup. The eddy is damped

because of two processes: interaction with the turbulent viscosity and the interaction with the source (microscopic viscosity is not considered here since in stars $\nu << \nu_t$). One can envisage the eddy as being "scattered" by "collisions" with the smaller eddies (turbulent viscosity) and by the source that drives energy into the eddy. The effective rate for the breakup (the inverse of the correlation timescale) will be taken to be the sum of the rates for the two processes as if they were operating independently: $\nu_t(k)k^2 + n_s(k)$, plus the sum of the rates for each process which is now affected by the other. Between "collisions" due to one process there is a random walk due to "collisions" of the other process. Thus, these last two rates are $n_s(\nu_t k^2/n_s)^{1/2}$ and $\nu_t k^2 (n_s/(\nu_t k^2))^{1/2}$. Summing up the four rates we obtain

$$\gamma n_c^*(k) = \nu_t(k)k^2 + n_s(k) + 2\left(\nu_t(k)k^2 n_s(k)\right)^{1/2} = \left(\left(\nu_t(k)k^2\right)^{1/2} + n_s(k)^{1/2}\right)^2 \qquad (31)$$

where γ is a proportionality constant, determined by the normalization of $y(k)$ in the inertial range. In this range equations (20), (29) and (31) yield

$$y(k) = \gamma^{-1}\left(\nu_t(k)k^2\right)^2 \qquad (32)$$

while equation (18) results in

$$\epsilon = y(k)\nu_t(k) \qquad (33)$$

with $\epsilon = \epsilon(\infty)$ where

$$\epsilon(k) = \int_{k_0}^{k}\left(n_s(k') + \nu k'^2\right)F(k')dk' = \left(\nu + \nu_t(k)\right)y(k) \qquad (34)$$

is the energy rate per unit mass supplied to the turbulence from the driving source at all wavenumbers smaller than k. Combined together, equations (32) and (33) imply that

$$y(k) = \epsilon^{2/3}\gamma^{-1/3}k^{4/3} \ . \qquad (35)$$

This should coincide with $y(k)$ corresponding to the Kolmogorov spectral function

$$y_K(k) = \frac{3}{2}K_O\epsilon^{2/3}k^{4/3} \ . \qquad (36)$$

Thus, we obtain

$$\gamma = \left(\frac{2}{3K_O}\right)^3 = 0.0878\left(\frac{K_O}{1.5}\right)^{-3} \qquad (37)$$

where K_O is the Kolmogorov constant. We used here the same normalization with respect to K_O as was used in CM (1991).

With the definition of $n_c^*(k)$, equation (31), the model equations can be solved for $F(k)$, and consequently for $G(k)$ and $H(k)$. We introduce for notational convenience (following the convention of CGC (1987)) the rate $n_c(k)$ defined by

$$\nu_t k^2 = \gamma n_c(k) \ . \tag{38}$$

In the model for large scale turbulence of Canuto & Goldman (1985) n_c^* was identified with n_s, neglecting the role of the turbulence. In CGC (1987) $n_c^* = n_c$ was used, neglecting the role of the source. Here, n_c^* depends both on n_s and on n_c, as seen from equations (31) and (38), so it depends both on the source and on the turbulence. At k_0, $n_c^* = 4n_c$ and therefore is 4 times larger than in CGC (1987). For high values of k (practically few times k_0) $n_c^* \to n_c$. It is of interest to note that the inverse of the timescale for two-times velocity correlation according to the DIA model, indeed conforms to the present definition of n_c^* (see figures 3 and 4 in Canuto & Battaglia 1988). In particular at k_0 it is indeed $\sim 4\,n_c$.

2.3. Differential Equation, Spectral Function, and Convective Flux

From equations (29) and (38) we have

$$F(k) = -\gamma n_c^*(k) \left(\frac{n_c}{k^2}\right)' \ , \tag{39}$$

and equations (20) and (38) lead to

$$y(k) = n_c^*(k)\Big(\gamma n_c(k) - n_s(k)\Big) \ . \tag{40}$$

Combining equations (39), (40) and (9) yields the differential equation for $n_c(k)$

$$2n_c^*(k)n_c'(k) + n_c^*(k)'\Big(n_c(k) - \gamma^{-1}n_s(k)\Big) - \gamma^{-1}n_c^*(k)n_s'(k) - 2n_c(k)n_c^*(k)\frac{1}{k} = 0 \tag{41}$$

with $n_s(k)$ and $n_c^*(k)$ defined as functionals of $n_c(k)$ through equations (28) and (31), respectively. A solution for $n_c(k)$ will also yield these two rates, as well as the spectral function $F(k)$ and the mean squared turbulent vorticity $y(k)$.

The main objective of this work is the computation of the turbulent convective flux

$$F_c = c_p \rho \overline{u_3 \theta} = c_p \rho \int_{k_0}^{\infty} H(k) dk = c_p \rho \beta \chi \Phi \ . \tag{42}$$

Here u_3 is the turbulent velocity in the flux direction, θ is the temperature fluctuation, and the overline denotes ensemble averaging. The dimensionless convective flux Φ is determined by equations (12) and (34) to be

$$\Phi = \epsilon (g \alpha \beta \chi)^{-1} \ . \tag{43}$$

The value of ϵ will be determined by using the fact that $\epsilon(k)$ increases with k and reaches its asymptotic value already in the inertial range. Thus, we shall follow the solution of $n_c(k)$ and the corresponding $\epsilon(k)$, from k_0 up to to the inertial range, until $\epsilon(k)$ saturates to ϵ. From equations (34), (38) and (40) we find

$$\epsilon(k) = n_c^*(k) \left(\nu + \frac{\gamma n_c(k)}{k^2} \right) \left(\gamma n_c(k) - n_s(k) \right) \ . \tag{44}$$

thus, once $n_c(k)$ is obtained, $\epsilon(k)$ is determined too.

3. Solution Procedure

Turn now to the equation (41) which is a first order differential equation for $n_c(k)$ and thus a boundary value is required for a unique solution. Below we find the value of $n_c(k_0)$. The value of k_0 is determined by the width of the layer Λ,

$$k_0 = \frac{\pi}{\Lambda} (1 + x_0)^{1/2} \tag{45}$$

with $x_0 \equiv x(k_0)$. Since by definition $F(k_0) = 0$ and $y(k_0) = 0$, equations (39), and (40) imply that

$$\gamma n_c(k_0) = n_s(k_0) = \nu_t(k_0) k_0^2 \tag{46}$$

and

$$\left(\frac{n_s}{k^2} \right)'_{k_0} = \left(\frac{\gamma n_c}{k^2} \right)'_{k_0} = 0 \ . \tag{47}$$

The last two equations together with equation (28) determine $n_c(k_0)$

$$\gamma n_c(k_0) = \sigma_t \chi k_0^2 z_0 \ , \tag{48}$$

where z_0 is the solution of

$$\left(\frac{\sigma}{\sigma_t} + z_0\right)^2 \left(1 + z_0^2\right) = \frac{x_0}{1 + x_0}\sigma_t^{-2}S_1^2 \ . \tag{49}$$

with

$$S_1 = \pi^{-4}(1 + x_0)^{-2}S = 0.0045627S \ , \tag{50}$$

where S is the dimensionless product of the Rayleigh and Prandtl numbers

$$S = \frac{g\alpha\beta\Lambda^4}{\chi^2} \ . \tag{51}$$

S, or more precisely S_1, is a measure of the convective efficiency. With the determination of $n_c(k_0)$, equation (41) can be solved numerically to yield $n_c(k)$ for any value of S.

Since we deal with stellar interiors for which $\sigma = \nu\chi^{-1} << 1$, we take in all the equations the limit of $\nu \to 0$. Physically this means that the wavenumber at which the rate of dissipation by the microscopic viscosity becomes equal to $\gamma n_c(k)$, is much larger than k_0, so that the spectrum exhibits an inertial range over many decades of k. For the limit of $\nu \to 0$, appropriate for stellar interiors, equation (49) yields an analytic solution for z_0 as function of S,

$$z_0 = \frac{2^{1/2}\sigma_t^{-1}\tau(1)S_1}{\sqrt{1 + \sqrt{1 + 4S_1^2\tau^2(1)\sigma_t^{-2}}}} \tag{53}$$

implying that

$$\gamma n_c(k_0) = n_s(k_0) = (g\alpha\beta)^{1/2}\eta_0(S) = \frac{\chi}{\Lambda^2}S^{1/2}\eta_0(S) \tag{54}$$

with

$$\eta_0(S) = \frac{2^{1/2}\tau(1)S_1^{1/2}}{\sqrt{1 + \sqrt{1 + 4S_1^2\tau^2(1)\sigma_t^{-2}}}} \tag{55}$$

and $\tau(1) = x_0(1 + x_0)^{-1}$. It is convenient to express the equations in terms of normalized rates

$$\eta_s(k) = \frac{n_s(k)}{n_s(k_0)} \; , \tag{56}$$

$$\eta_c(k) = \frac{\gamma n_c(k)}{n_s(k_0)} \tag{57}$$

and

$$\eta_c^*(k) = \frac{\gamma n_c^*(k)}{n_s(k_0)} \tag{58}$$

and to introduce a dimensionless wavenumber

$$q = \frac{k}{k_0} \; . \tag{59}$$

Using equations (26), (27) and (28) in equation (47) results in

$$\left(\frac{\tau(k)}{k^4} \right)'_{k_0} = 0 \tag{60}$$

We adopt, following CGC (1987),

$$x(k) = \left(\frac{k\Lambda}{\pi} \right)^2 - 1 \tag{61}$$

for which equation (60) yields

$$k_0 = \left(\frac{3}{2} \right)^{1/2} \frac{\pi}{\Lambda} \tag{62}$$

Thus

$$\tau(q) = 1 - \frac{2}{3q^2} \tag{63}$$

and

$$x_0 = \frac{1}{2} \tag{64}$$

The differential equation for $\eta_c(q)$ is obtained from equation (41)

$$2\eta_c^*(q)\eta_c'(q) + \eta_c^*(q)'(\eta_c(q) - \eta_s(q)) - \eta_c^*(q)\eta_s'(q) - 2\eta_c(q)\eta_c^*(q)\frac{1}{q} = 0 \ , \tag{65}$$

where now the prime denotes differentiation with respect to q. By definition [see eqns. (56), (57), (58)]

$$\eta_c(q = 1) = \eta_s(q = 1) = 1 \quad ; \quad \eta_c^*(q = 1) = 4 \ , \tag{66}$$

for any S. We have now

$$\eta_s(q) = \frac{S_1^{1/2}\eta_0^{-1}\tau(q)B(q)}{2q^2 A(q)} \tag{67}$$

where

$$A(q) = \left(1 + \frac{S_1\eta_0^2\eta_c^2(q))}{\sigma_t^2 q^4}\right)^{3/2} \ , \tag{68}$$

and

$$B(q) = 1 + \left(1 + \frac{4S_1^{1/2}\eta_0^3 A(q)\eta_c^3(q))}{\sigma_t^2 \tau(q)q^2}\right)^{1/2} \ . \tag{69}$$

The use of the normalized rates ensures that the computed quantities will not be very small (large) even for very small (large) S values, thus improving the numerical accuracy. Equation (44) becomes now,

$$\epsilon(q) = \frac{1}{\gamma}(g\alpha\beta\chi)\eta_0^3 S_1^{1/2} q^{-2}\eta_c(q)\eta_c^*(q)\Big(\eta_c(q) - \eta_s(q)\Big) \tag{70}$$

the dimensionless convective flux is given by

$$\Phi(S) = \frac{1}{\gamma}\eta_0^3 S_1^{1/2} q_f^{-2}\eta_c(q_f)\eta_c^*(q_f)\Big(\eta_c(q_f) - \eta_s(q_f)\Big) \tag{71}$$

where q_f is the upper value of q for which equation (65) is solved, and is well inside the inertial range (thus, $\epsilon(q_f) = \epsilon$).

4.   Results

4.1.   Convective Flux

We solved equation (65) for $\eta_c(q)$, with the initial condition of equation (66), for S in the range 10^{-4}—10^{20} . We adopted the commonly used value of $\sigma_t = 0.72$. Each solution yields $\eta_s(q)$ and $\eta_c^*(q)$ and the spectral function $F(q)$. For each such solution we computed $\epsilon(q)$, followed it to saturation, and thus obtained $\epsilon(S)$ and $\Phi(S)$.

In Figure 1 we show $\epsilon(q)$ in units of $(K_O/1.5)^3 g\alpha\beta\chi$, for $S = 10^6$. The qualitative behavior of $\epsilon(q)$ is typical for any value of S: it starts from zero and saturates in the inertial range to ϵ. From equations (70) and (71) it follows that the asymptotic value of the graph equals Φ in units of $(K_O/1.5)^3$.

In Table 1 we list $\Phi(S)$ (rounded to 4 figures) for 20 representative values of S. From equation (71) it follows that $\Phi(S) \propto \gamma^{-1} \propto K_O^3$. The values shown in Table 1 are in units of $(K_O/1.5)^3$. The limiting behavior of $\Phi(S)$ is given by

$$\Phi = 2.65 \times 10^{-5} \left(\frac{K_O}{1.5}\right)^3 S^2 \quad ; \quad S << 1 , \tag{72}$$

and

$$\Phi = 1.6853 \left(\frac{K_O}{1.5}\right)^3 \left(\frac{\sigma_t}{0.72}\right)^{3/2} S^{1/2} \quad ; \quad S >> 1 . \tag{73}$$

In applications of $\Phi(S)$ to stellar structure codes, it is useful to have an analytic fit formula to the convective flux. We derived such a fit with a deviation $\lesssim 3\%$:

$$\Phi = F_1(S) F_2(S) \tag{74}$$

where

$$F_1(S) = \left(\frac{K_O}{1.5}\right)^3 a\, S^k \Big((1 + b\, S)^m - 1\Big)^n \tag{75}$$

where

$$a = 10.8654 \,, b = 0.00489073 \,, k = 0.149888 \,, m = 0.189238 \,, n = 1.85011$$

and

Table 1.   The Results of the Model

S	Φ	$\frac{\Phi}{\Phi_{MLT}}$	$\frac{\Phi}{\Phi_{CM}}$	$\overline{v^2}$	p_t	C
10^{-4}	2.65×10^{-13}	0.3091	2.814	2.112×10^{-11}	5.3408×10^{-12}	0.2529
0.01	2.65×10^{-9}	0.3092	2.814	2.112×10^{-7}	5.341×10^{-8}	0.2529
1.	2.65×10^{-5}	0.3148	2.819	2.112×10^{-3}	5.341×10^{-4}	0.2529
10	2.649×10^{-3}	0.3663	2.863	0.2111	0.5339	0.2529
30	2.38×10^{-2}	0.4811	2.96	1.895	0.4793	0.2529
10^2	0.2557	0.8745	3.203	20.52	5.186	0.2527
300	1.88	1.806	3.409	157.6	39.63	0.2515
10^3	10.23	3.334	3.045	1.019×10^3	252.4	0.2478
10^4	85.01	5.82	2.065	1.685×10^4	4.017×10^3	0.2384
10^5	388.5	7.381	1.59	1.954×10^5	4.515×10^4	0.2311
10^6	1.442×10^3	8.312	1.348	2.049×10^6	4.648×10^5	0.2268
10^7	4.917×10^3	8.849	1.209	2.085×10^7	4.680×10^6	0.2245
10^8	1.615×10^4	9.155	1.125	2.094×10^8	4.687×10^7	0.2238
10^9	5.21×10^4	9.326	1.072	2.099×10^9	4.688×10^8	0.2233
10^{10}	1.665×10^5	9.42	1.038	2.101×10^{10}	4.688×10^9	0.2231
10^{12}	1.679×10^6	9.498	1.001	2.101×10^{12}	4.688×10^{11}	0.2231
10^{14}	1.684×10^7	9.528	0.9863	2.101×10^{14}	4.689×10^{13}	0.2231
10^{16}	1.685×10^8	9.534	0.9795	2.101×10^{16}	4.689×10^{15}	0.2231
10^{18}	1.685×10^9	9.534	0.9764	2.101×10^{18}	4.689×10^{17}	0.2231
10^{20}	1.685×10^{10}	9.534	0.9751	2.101×10^{20}	4.689×10^{19}	0.2231

Φ is in units of $(K_O/1.5)^3$ and its high S limit scales as $(\sigma_t/0.72)^{3/2}$. $\overline{v^2}$ and p_t are in units of $\left(\frac{\chi}{\Lambda}\right)^2 \left(\frac{K_O}{1.5}\right)^3$ and $\rho \left(\frac{\chi}{\Lambda}\right)^2 \left(\frac{K_O}{1.5}\right)^3$, respectively. Their high S limits scale as $(\sigma_t/0.72)$. The dimensionless ratio, C, is defined in equation (88).

$$F_2(S) = 1 + \frac{c\,S^p}{1 + d\,S^q} + \frac{e\,S^r}{1 + f\,S^t} \ , \tag{76}$$

where

$$c = 0.0108071 \ , d = 0.00301208 \ , e = 0.000334441 \ , f = 0.000125 \ ,$$

$$p = 0.72 \ , q = 0.92 \ , r = 1.2 \ , t = 1.5 \ .$$

In order to judge the quality of the fit, in Figure 2 we display the ratio between the fit function and an interpolation of the numerical values, as a function of $\log S$.

Also shown in Table 1 are the ratios $\Phi(S)/\Phi_{MLT}(S)$ and $\Phi(S)/\Phi_{CM}(S)$ where Φ_{MLT} and Φ_{CM} are the values corresponding to the MLT,

$$\Phi_{MLT}(S) = \frac{729}{16}S^{-1}\left(\left(1 + \frac{2}{81}S\right)^{1/2} - 1\right)^3 \ , \tag{77}$$

and to the CM model (their eq. [32]). Figures 3 and 4 display $\Phi(S)/\Phi_{MLT}(S)$ and $\Phi(S)/\Phi_{CM}(S)$, respectively. Note that the qualitative behavior of $\Phi(S)/\Phi_{MLT}(S)$ is similar to that of the CM model—higher flux for high S and lower flux for low S values. The comparison with $\Phi_{CM}(S)$ shows that while the two models yield essentially the same flux for high S values, the new model predicts higher fluxes for intermediate and low S values, and the flux ratio is maximal for $S \sim 300$. Comparisons of $\Phi(S)$ computed within the new model with $\Phi(S)$ computed in a model with the same definition of n_c^* but with n_s equal to the linear growth rate, indicates that the above local maximum at $S \sim 300$ is a feature resulting from the use of the selfconsistent rate. We recall that $S_1 = 0.0045627\,S$ rather than S is the measure of the convective efficiencies. Thus, the borderline between low and high efficiencies is around $S = 300$, which is also where the ratio of the new convective flux to that of the CM model is maximal.

4.2.   Turbulent Velocity, Turbulent Pressure and Turbulent Viscosity

The mean squared turbulent velocity is defined by

$$\overline{v^2} = \int_{k_0}^{\infty} F(k)dk \tag{78}$$

which with the use of equation (39) can be expressed as

$$\overline{v^2} = \chi^2 \Lambda^{-2} \gamma^{-1} \frac{1}{\pi^2(1+x_0)} S \eta_0^2(S) \int_1^\infty f(q) dq \ , \tag{79}$$

with

$$f(q) = -\eta_c^*(q) \left(\frac{\eta_c(q)}{q^2} \right)' \ . \tag{80}$$

We computed $\overline{v^2}$ for each value of S and the results are presented in Table 1. The limiting behavior is given by

$$\overline{v^2} = 2.1117 \times 10^{-3} \left(\frac{K_O}{1.5} \right)^3 \left(\frac{\chi}{\Lambda} \right)^2 S^2 \quad ; \quad S << 1 \tag{81}$$

and

$$\overline{v^2} = 2.10146 \left(\frac{K_O}{1.5} \right)^3 \left(\frac{\sigma_t}{0.72} \right) \left(\frac{\chi}{\Lambda} \right)^2 S \quad ; \quad S >> 1 \tag{82}$$

The turbulent pressure is of importance in helioseismological models. Batchelor (1953) derived an expression for the mean squared turbulent pressure (for the case of isotropic turbulence) in terms of the spectral function $F(k)$

$$p_t^2 = \frac{1}{4} \rho^2 \int_{k_0}^\infty \int_{k_0}^\infty F(k) F(k') I(k/k') dk' dk \tag{83}$$

where ρ is the mean density and the dimensionless integral $I(x)$ is

$$I(x) = I(1/x) = \frac{1}{2} \left(x^2 + x^{-2} \right) - \frac{1}{3} - \frac{1}{4} \left(x + x^{-1} \right) \left(x - x^{-1} \right)^2 \ln \frac{1+x}{|1-x|} \ . \tag{84}$$

$I(x) \to 0$ for $x \to 0\,, \infty$ and is maximal at $x = 1$, where it equals $2/3$. Thus, the pressure is mostly contributed by $k' \sim k$ which are close to the maximum of $F(k)$. Using equation (39) we obtain

$$p_t^2 = \frac{1}{4\gamma^2} \rho^2 \chi^4 \Lambda^{-4} \frac{1}{\pi^4(1+x_0)^2} S^2 \eta_0^4(S) \int_1^\infty \int_1^\infty f(q) f(q') I(k/k') dq' dq \ . \tag{85}$$

The computed values of the root mean squared turbulent pressure are displayed in Table 1. The asymptotic behavior is given by

$$p_t = 5.3408 \times 10^{-4} \rho \left(\frac{\chi}{\Lambda}\right)^2 \left(\frac{K_O}{1.5}\right)^3 S^2 \quad ; \quad S << 1 \tag{86}$$

and

$$p_t = 0.4689 \rho \left(\frac{\chi}{\Lambda}\right)^2 \left(\frac{K_O}{1.5}\right)^3 \left(\frac{\sigma_t}{0.72}\right) S \quad ; \quad S >> 1 . \tag{87}$$

A quantity of interest is $C(S)$ defined as

$$C(S) = \frac{p_t}{\rho \overline{v^2}} \tag{88}$$

The computed values of C are listed in Table 1. As can be seen, it is almost constant for all values of S, ranging from 0.253 for low S to 0.223 for high values of S.

As with the convective flux it is useful to have analytical fit formulae for the mean squared turbulent velocity and for the root mean squared turbulent pressure. We derived such fits which represent the numerical values with precision better than 3%. For the mean squared velocity we derive the fit

$$v^2 = \left(\frac{\chi}{\Lambda}\right)^2 F_3(S) F_4(S) , \tag{89}$$

where

$$F_3(S) = \left(\frac{K_O}{1.5}\right)^3 \frac{0.00101392 \, S^2}{1 + \sqrt{1 + 0.000017848 \, S^2}} \tag{90}$$

and

$$F_4(S) = 6.39899 + \frac{2.256815 \left(-1. + 0.000777055 \, S^{0.868589}\right)}{1. + 0.000777055 \, S^{0.868589}} . \tag{91}$$

Similarly, for the root mean square of the turbulent pressure we find

$$p_t = \rho \left(\frac{\chi}{\Lambda}\right)^2 F_3(S) F_5(S) \tag{92}$$

with $F_3(S)$ given by equation (90) and

$$F_5(S) = 1.49168 + 0.45185 \frac{-1. + 0.00111378 \, S^{0.868589}}{1. + 0.00111378 \, S^{0.868589}} . \tag{93}$$

Finally, the turbulent viscosity, is given in the present model already in an *analytic* form. From equations (38), (44), (45), (54) and (55) we find that

$$\nu_t \equiv \nu_t(k_0) = \chi \frac{0.00215086\,S}{\sqrt{1 + \sqrt{1 + 0.000017848\,S^2}}}\ . \tag{94}$$

The limiting behavior of ν_t is given by

$$\nu_t = 0.00152089\,\chi\,S \quad ; \quad S << 1 \tag{95}$$

and

$$\nu_t = 0.03309\,\chi\,S^{1/2} \quad ; \quad S >> 1. \tag{96}$$

5. Application to stellar models

The new convective fluxes have been included in the ATON stellar structure code (for an update on the physical and numerical details of the code, see Mazzitelli et al. 1995 and references therein). We have computed the main sequence evolution of a solar model as well as a set of evolutions for Pop II stars having $M \leq 0.9 M_\odot$, from the zero age main sequence to the base of the red giant phase.

Before turning to a detailed discussion of the results, we recall that, the turbulent length-scale Λ at a given depth z inside a convective region, must also include the thickness OV of the overshooting layers (if any) beyond the formal Schwarzschild boundary (see D'Antona and Mazzitelli 1994). At present, the OV phenomenon has not yet been fully quantified in a reliable way (Umezu 1995) even though the underlying equations have been derived (Canuto 1993). However, empirical evidence from comparisons between stellar models constructed with local convection theories, and observations of intermediate mass main sequence stars in young open clusters, suggests quite stringent limits on the extent of the OV, namely, $0 \leq OV \leq 0.2 H_p$ (Stothers & Chin 1992). Lacking a formal theory, we shall write

$$\Lambda = z + \alpha^* H_p^{top}\ . \tag{97}$$

where H_p^{top} is the pressure scale height at the upper boundary of the convective layer determined by the Schwarzschild criterion and α^*, which should not exceed 0.2, can be regarded as a *fine-tuning* parameter.

We stress that the role of α^* in the CM and in the present models is *radically* different from the role of the parameter α in the MLT model where $\Lambda = \alpha H_p(z)$. In fact, α is a free adjustable parameter through which modelists try to capture all the physical uncertainties (e. g. opacities, convection, thermodynamics etc.) relevant to the evaluation of the effective temperatures of stars . Unfortunately, not only does this procedure seriously hinder the predictive power of stellar modeling (α is determined *a posteriori*), but the fit to the observed surface temperature does not automatically guarantee that also the *internal temperature profile* is correct. In this context, it is worth noting that Baturin & Mironova (1995) and Monteiro et al. (1995) have recently shown that the solar internal temperature profiles predicted by the CM model are in better agreement with helio-seismological data than those derived from the MLT. Moreover, Gabriel (1995) has shown that the MLT could be made to predict a CM-like internal temperature profile, provided that α is *forced to vary inside the convective region*, in a manner that represents an a posteriori fitting. This quite clearly shows that a) the MLT has no predictive power and b) the degree of artificiality that is required to make the MLT yield results that the CM model produces quite naturally. The parameter α^*, on the other hand, quantifies a well identified *physical process*, the convective overshooting OV and, as seen in the following, in the present model, only a marginal amount of tuning is allowed anyhow.

Finally, the convective flux in Table 1 is normalized to a value of the Kolmogorov constant of $K_O = 1.5$, as in the CM model. Since recent experimental data suggest higher values of K_O (up to ~ 1.9), we employed for the stellar modeling a fiducial value of $K_O = 1.7$ in the fit-formula, equation (75). Since, as discussed in §4.1, the convective flux scales as K_O^3, the flux used is a factor of $(1.7/1.5)^3$ larger than the numerical values in Table 1. In Mazzitelli et al. (1995) $K_O = 1.8$ was used.

Using the ATON code, and updating the low–T opacities according to Alexander and Ferguson (1994), we obtained a fit to the observed solar radius and luminosity at an age ~ 4.55 Gyr (Bahcall 1989), and with a metal abundance Z=0.0175 (Grevesse and Noels 1993), with Y$\sim$0.27 and $\alpha^* \sim 0.08$. The latter corresponds to a very small amount of overshooting of a *few kilometers*, and is in full accordance with the observational limits of Stothers & Chin (1992). On the other hand, had we employed the original CM model the required value would have been $\alpha^* \sim 0.2$ which is a borderline value. To find the maximal variance in T_{eff} allowed by the α^* parameter, we computed two solar models with the borderline values $\alpha^* = 0$ and $\alpha^* = 0.2$. The difference in T_{eff} between these last two models turned out to be $<4\%$.

Figure 5 shows the internal profiles of the dimensionless temperature gradient, $d\log T/d\log P$, in the region of the overadiabaticity peak for solar models computed with

the present, the CM and MLT models (for the MLT model $\alpha = 1.55$). The results of the present model are very similar to those of the CM model but are quite different from the MLT results. The similarity of the results of the present and CM models, in spite of the difference (factor ~ 3) in the value of the convective flux for intermediate and low convective efficiencies, can be readily understood. In the more external convective layers, the density is quite low ($\rho \leq 10^{-7}$), and $\mathrm{Log}\,S < 2$. The turbulent flux is also quite low, and convective energy transfer is very inefficient. Most of the flux in this region is therefore carried by radiation, and the temperature gradient sticks to the radiative one. In deeper convective layers, where ρ, S and Λ are larger, convection begins to be efficient and the value of the temperature gradient is determined by the turbulent convective flux. However, for S values such that $\mathrm{Log}\,S \gg 3$, the new fluxes are very close to the CM ones, and so is the resulting temperature gradient. The vicinity of the gradient peak, $\mathrm{Log}\,S \sim 2$, is close to the S value where the present and CM models differ the most (see Fig. 3). Thus, this is the region where we can expect some sizable difference between the temperature profiles, as Figure 5 indeed shows.

Because of the similarity of the results from the present and the CM models, the experimental benchmark provided by helioseismological data cannot discriminate between the two models (Antia and Basu 1995). However, on the basis of stellar modeling, we stress that the new fluxes require a lower value of α^* to fit the sun, which is more in agreement with the results of Stothers & Chin. Since the low–T radiative opacities are probably still slightly underestimated, and larger opacities require a larger α^* to fit the sun, we prefer the present new fluxes over the original CM values. The reason is that the latter, once the updated values of low–T opacities become available, could require values of α^* larger than allowed by the observational upper limit on overshooting.

As a further check, we have also applied the new fluxes to the computation of evolutionary tracks and isochrones for stars with $Y = 0.23$ and $Z = 10^{-4}$. The isochrones are shown in Figure 6, together with the fiducial sequence of the globular cluster M68. Details on the computations of both tracks and isochrones, on the observational to theoretical correlations, as well as the chemistry, reddening and distance modulus for M68 can be found in Mazzitelli et al. (1995). Here we simply recall that the apparent "kinks" in the isochrones are a true physical feature, which is expected and explained within the CM framework, and which exists also in the present model.

The age of the cluster is in the range $11 \div 12$ Gyr, somewhat younger than the $12 \div 13$ Gyr found with the CM fluxes, which itself is younger than the $13 \div 15$ Gyr derived within the MLT. Whether this difference is significant for solving the age conflict of globular clusters with the age of the universe, following from the recent determinations of high values

of H_0 (Freedman et al. 1994, Pierce et al. 1994), is beyond the purposes of the present paper. This point will be discussed elsewhere (Canuto et al. 1996).

In conclusion, the application of the convective fluxes of the present model to stellar structure does not alter appreciably the main results of the CM model. Nevertheless, the new model is preferable on two grounds. From the theoretical viewpoint, it determines the rate of input of energy from buoyancy to the turbulence in a more physically consistent manner. From the astrophysical point of view, it requires a smaller extent of overshooting, which is in better agreement with recent observational results.

6. Discussion

We have presented a selfconsistent model for turbulent convection based on a simplified treatment of the non-linear interactions among the eddies. The important novel feature of the present model is the formulation of a selfconsistent rate for energy input from the *source* (buoyancy) into the turbulence, which depends both on the source parameters and on the *turbulence* itself. This represents an improvement compared to the CM model where the rate of energy input was the growth rate of the *linear* unstable modes. The focus of the present model is on the selfconsistent rate of energy input at the expense of a less complete treatment of the non-linear eddy interactions. The latter is much simpler than in the CM model and describes transfer only from small to large wavenumbers. This representation neglects non-local (in k space) interactions between the eddies that lead to a reverse transfer (backscatter) that are included in the CM model.

We have explored the model for a wide range of convective efficiencies and computed, numerically, the dimensionless convective flux, the turbulent squared velocity and the root mean squared turbulent pressure, as functions of the convective efficiency S. The results were fitted by analytical formulae with precision better than 3% over the range $S = 10^{-4} \div 10^{20}$. The turbulent viscosity in the model is already given by an analytic expression. The convective flux, is larger than that of the MLT for high convective efficiencies and lower than it for low convective efficiencies. This general behavior is similar to that of the CM model. The high S fluxes are very close to those predicted by the CM model but the intermediate and lower S fluxes are larger than those of the CM model.

It is of interest to note that even the very simple CGC (1987) model shares the same qualitative behaviour of the convective flux relative to that of the MLT flux, as function of the convective efficiency. The fact that three models differing in their treatment of the energy input rate and in the modeling of the nonlinear transfer, still yield the same

behaviour is quite intriguing. It suggests that accounting for the full turbulence spectrum (common to all three models) is far more important than the detailed way in which thye latter is done.

We have applied the new model to the main sequence evolution of a solar model as well as to evolutions of POP II stars with $M \leq 0.9 \; M_\odot$. The convective turbulent length scale was taken equal to the depth in the convective zone, as in the CM model. The results are generally similar to those of the CM model. However, the new model has the advantage that the overshooting required to fit the solar model is smaller than in the CM model. Also, the ages of globular clusters are smaller than the corresponding ages in the CM model by ~ 1 Gyr, which may help alleviate a possible conflict between the ages of globular clusters and a high value of H_0. As already noted in §5, the similarity between the temperature profiles for the solar model, predicted by the present and the CM models, renders the models practically indistinguishable by helioseismological data (Antia & Basu 1995). The situation is similar with regard to solar atmosphere modeling (Kupka 1995). However, atmospheres of cool stars are expected to yield observable differences between the two models (Kupka 1995).

From the theoretical perspective, a more complete model is one that incorporates a selfconsistent rate of energy input while keeping the non-linear interactions in their full generality, as done within the CM model. Work in this direction is in progress.

Finally, the present and the CM models are based on two-point correlations of the turbulent quantities. This methodology, preferred by the physics community, yields information about the spectral properties of the turbulence. Yet, its applicability to inhomogeneous and anisotropic cases is limited. An alternative approach, based on one-point correlation functions, is widely used in the engineering community and can handle anisotropy and inhomogeneity. While the spectral information is lost in this Reynolds Stress formalism, the method is easy to apply to non-local and space-dependent problems and has the potential to treat stellar convective overshooting (Canuto 1993). The method has already been successfully applied to the planetary boundary layer (PBL) which is the seat of strong convection (Canuto et al. 1994a) as well as to study the interaction between shear, vorticity and buoyancy at the surface of the sun (Canuto et al. 1994b). Work is in progress (Gabriel 1996, Houdeck 1996) to apply the same method to the study of helioseismology.

REFERENCES

Alexander, D.R. & Ferguson, J. W, 1994, ApJ, 437, 879

Althaus, L.G. & Benvenuto, O. G. 1996, MNRAS, 278, 981

Antia, H.M. & Basu, S. 1995, private communication

Batchelor, G. K. 1953, Theory of Homogeneous Turbulence (Cambridge: Cambridge Univ. Press)

Bahcall, J.N. 1989, Neutrino Astrophysics (Cambridge: Cambridge Univ. Press), 79

Baturin, V. A. & Mironova, I. V. 1995 AZh, 72, 120

Canuto, V. M. 1993, ApJ, 416 ,331

Canuto, V. M. & Goldman, I. 1985, Phys. Rev. Lett., 54, 430

Canuto, V. M., Goldman, I., & Chasnov, J. 1987, Phys. Fluids, 30, 3391

Canuto, V. M. & Battaglia, A. 1988, A&A, 193, 313

Canuto, V. M. & Mazzitelli, I. 1991, ApJ, 370, 295

Canuto, V. M., Cheng, Y., Hartke, G. J., & Schilling, O. 1991, Phys. Fluids A, 3, 1633

Canuto, V. M., Minotti, F. O., Ronchi, C., Ypma, R. M. & Zeman, O., 1994a, J. Atmos. Sci., 51, 1605

Canuto, V.M., Minotti, F. O. & Schilling, O. 1994b, ApJ, 425, 303

Canuto, V. M., Caloi, V., D'Antona F., & Mazzitelli I. 1996 ApJ, submitted

D'Antona F., & Mazzitelli I. 1994, ApJS, 90, 467

Freedman, W. L., Madore, B.F., Mould, R.J. et al. 1994, Nature, 371, 757

Gabriel, M. 1995, A&A, 302, 271

Gabriel, M. 1996, private communication

Grevesse, N., & Noels, A. 1993, in Origin and Evolution of the Elements, Eds. N. Prantzos, E. Vangioni-Flam, M. Cass (Cambridge: Cambridge Univ. Press), 14

Hartke, G. J., Canuto, V. M., & Dannevik, W. P. 1988, Phys. Fluids, 31, 256

Houdeck, G. 1996, private communication

Kupka, F. 1995, private communication

Mazzitelli, I., D'Antona, F. & Caloi, V. 1995, A&A, 302, 384

Monteiro, M.J.P.F.G., Christensen–Dalsgaard, J., & Thompson, M.J., 1995, in GONG 94: Helio and Asteroseismology from the earth and space, ASP Conf. Ser. 76, 128

Pierce, M.J., Welch, D.L., McClure, R.D. et al. 1994, Nature, 371, 385

Stothers, R.B. & Chin C-W. 1992, ApJ, 390, 136

Stothers, R.B. & Chin C-W. 1995, ApJ, 440, 297

Umezu, M. 1995, MNRAS, 276, 1287

Yamaguchi, S. 1963, PASJ, 15, 412
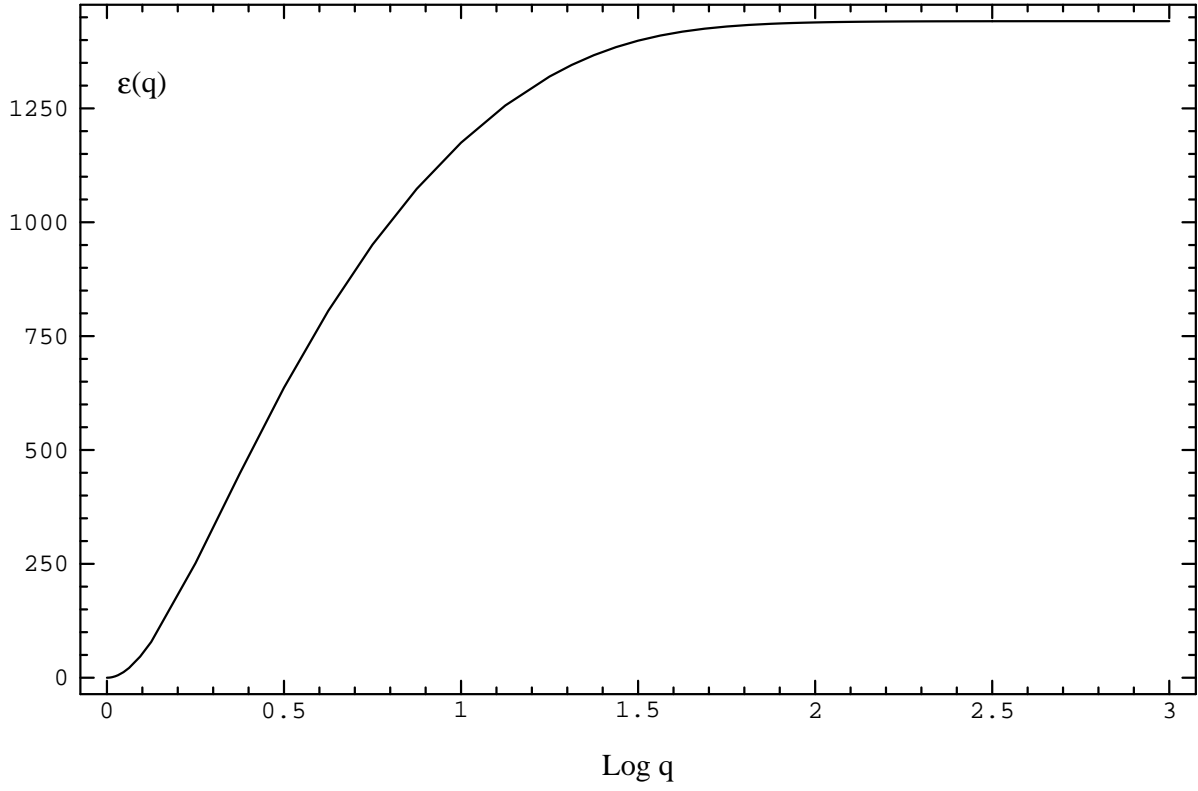
Fig. 1.— $\epsilon(q)$ in units of $(K_O/1.5)^3 g\alpha\beta\chi$, for $S = 10^6$. The asymptotic value shown is actually Φ in units of $(K_O/1.5)^3$.
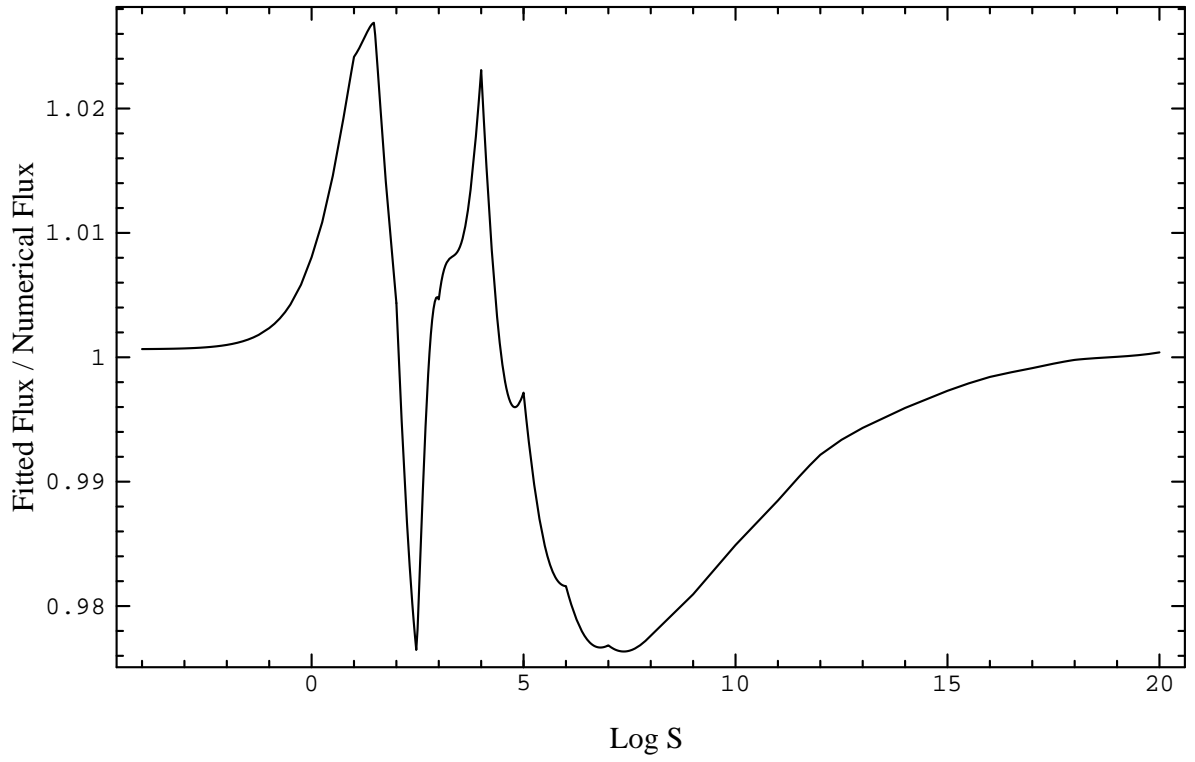
Fig. 2.— The ratio between the fit function for $\Phi(S)$, eq. (74), and an interpolation of the numerical values of $\Phi(S)$.
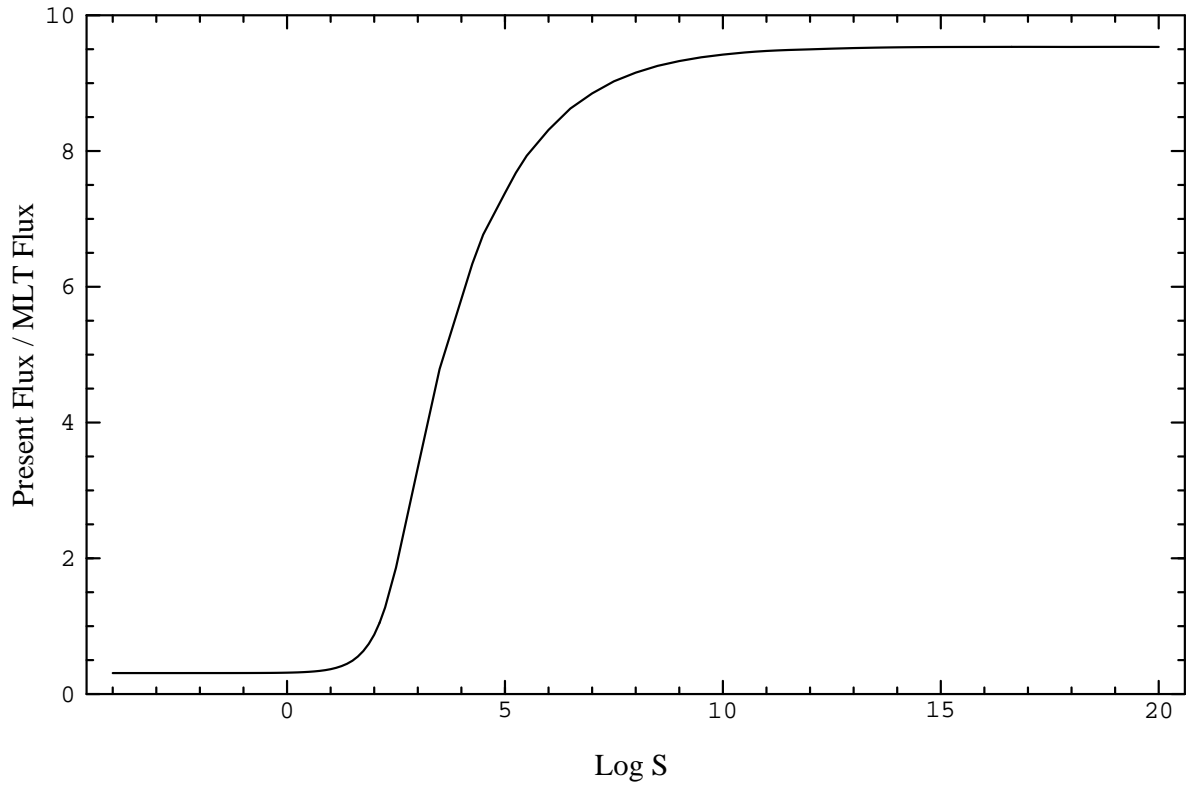
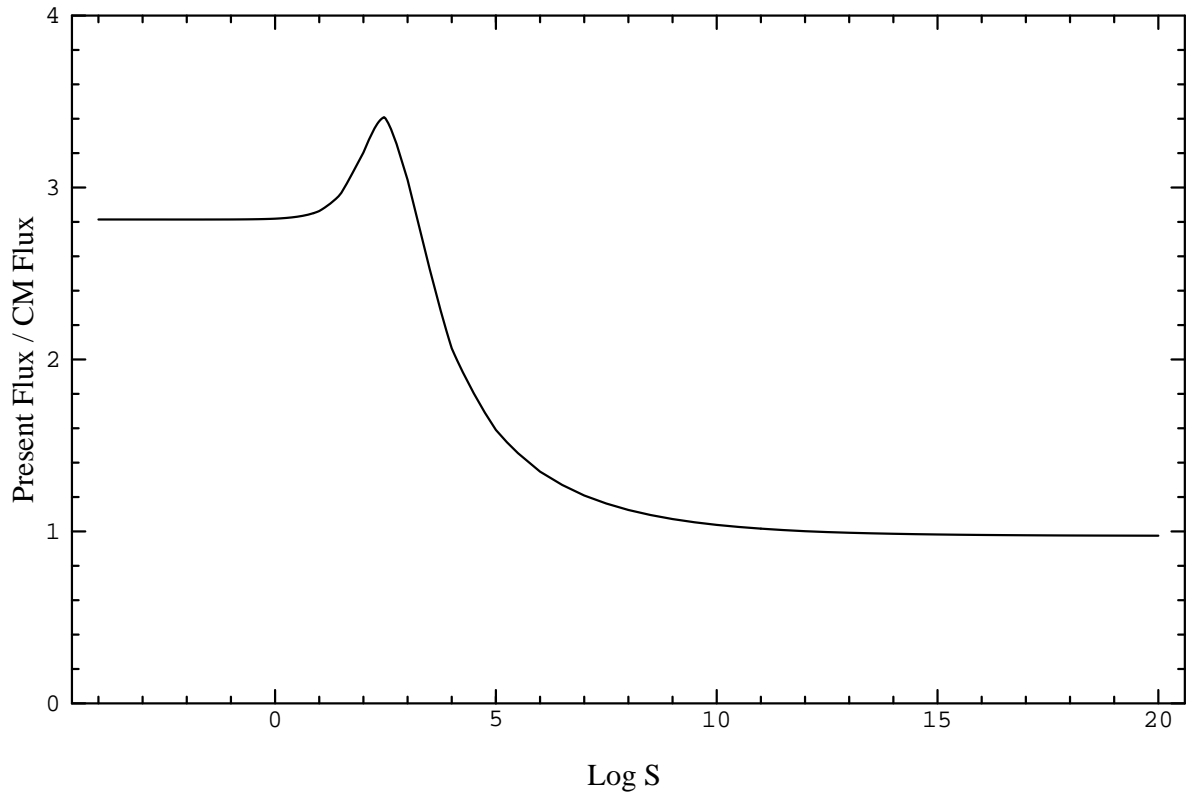Fig. 3.— The ratio $\Phi(S)/\Phi_{MLT}(S)$.
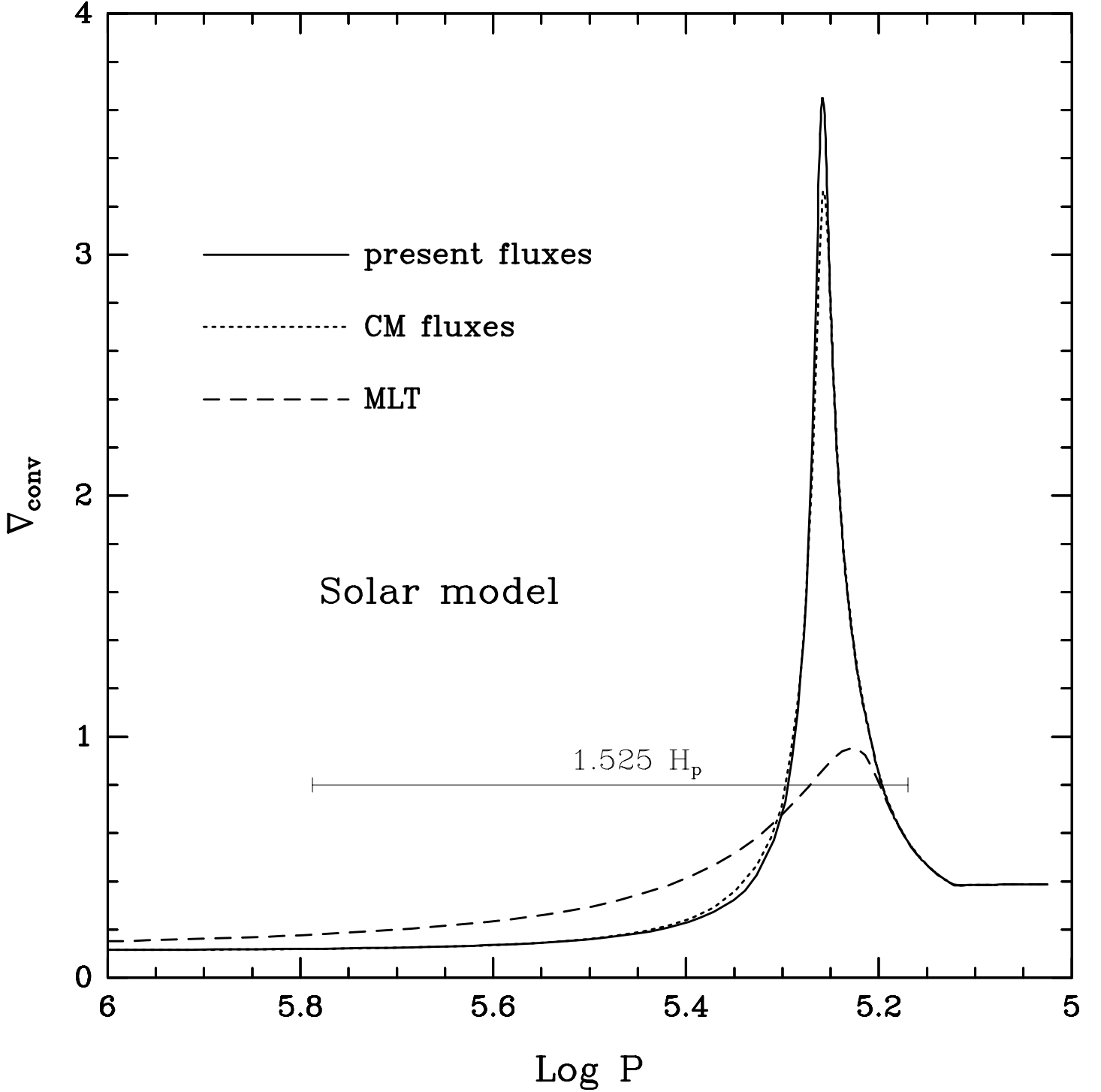
Fig. 4.— The ratio $\Phi(S)/\Phi_{CM}(S)$.

Fig. 5.— The dimensionless temperature gradient, $d\log T/d\log P$, versus pressure in the upper convective layer of the sun. The solid line corresponds to the present model. The dotted line corresponds to the CM model. The MLT (with $\alpha = 1.55$) yields quite different results represented by the dashed line.
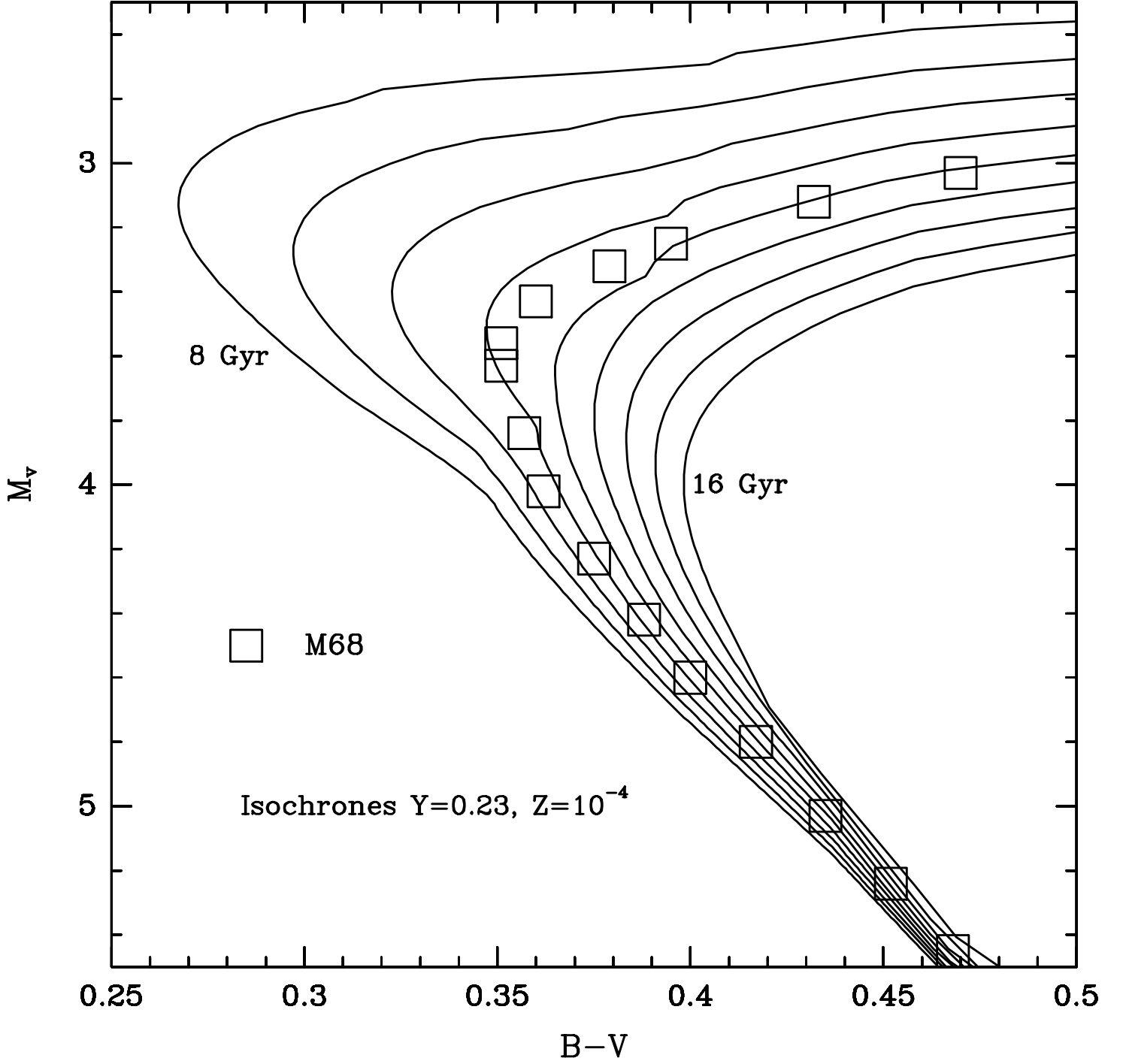
Fig. 6.— Isochrones in the HR diagram computed with the present model for an extreme
Pop II chemical composition ($Y = 0.23$ and $Z = 10^{-4}$). The squares mark the fiducial Turn
Off region for the very metal-poor globular cluster M68.